J Solid State Electrochem (2005) 9: 10–20
DOI 10.1007/s10008-004-0530-0

ORIGINAL PAPER

V. V. Kharton · E. V. Tsipis · I. P. Marozau
A. A. Yaremchenko · A. A. Valente · A. P. Viskup
J. R. Frade · E. N. Naumovich · J. Rocha

Transport and electrocatalytic properties of $La_{0.3}Sr_{0.7}Co_{0.8}Ga_{0.2}O_{3-\delta}$ membranes

Received: 13 November 2003 / Accepted: 18 March 2004 / Published online: 1 May 2004

Abstract Incorporation of gallium into the perovskite lattice of $La_{0.3}Sr_{0.7}CoO_{3-\delta}$ leads to increasing unit cell volume and to decreasing thermal expansion, total conductivity and oxygen permeability. At 973–1223 K, the oxygen permeation fluxes through $La_{0.3}Sr_{0.7}Co_{0.8}Ga_{0.2}O_{3-\delta}$ ceramics with 96.5% density are determined by the bulk ionic conduction and surface exchange rates. The total conductivity of $La_{0.3}Sr_{0.7}Co_{0.8}Ga_{0.2}O_{3-\delta}$, predominantly p-type electronic, exhibits an apparent pseudometallic behavior due to oxygen losses on heating, whereas the $p(O_2)$ dependencies of the conductivity and Seebeck coefficient suggest a small-polaron mechanism of hole transport. The average thermal expansion coefficients in air are 15.9×10^{-6} K^{-1} at 360–710 K and 27.9×10^{-6} K^{-1} at 710–1030 K. On decreasing oxygen pressure down to 4–30 Pa at 973–1223 K, perovskite-type $La_{0.3}Sr_{0.7}Co_{0.8}Ga_{0.2}O_{3-\delta}$ transforms into a brownmillerite-like modification, whose electrical properties are essentially $p(O_2)$ independent. Further reduction results in the decomposition of the brownmillerite into a multiphase oxide mixture at $p(O_2) = 8\times10^{-10}$–3×10^{-4} Pa, and then in the segregation of metallic cobalt. Due to surface-limited oxygen transport, $La_{0.3}Sr_{0.7}Co_{0.8}Ga_{0.2}O_{3-\delta}$ membranes are, however, kinetically stable under an air/CH_4 gradient up to 1223 K. The conversion of dry methane in model membrane reactors increases with oxygen permeation flux and temperature, but yields high CO_2 concentrations (>90%), indicating a dominant role of complete CH_4 oxidation on the membrane surface.

Keywords Perovskite · Oxygen membrane · Mixed conductor · Methane oxidation · Electron–hole transport

V. V. Kharton (✉) · E. V. Tsipis · A. A. Yaremchenko
J. R. Frade · E. N. Naumovich
Department of Ceramics and Glass Engineering, CICECO,
University of Aveiro, 3810-193 Aveiro, Portugal
E-mail: kharton@cv.ua.pt
Tel.: +351-234-370263
Fax: +351-234-425300

E. N. Naumovich · I. P. Marozau · A. P. Viskup
V. V. Kharton
Institute of Physicochemical Problems,
Belarus State University, 14 Leningradskaya Str.,
220050 Minsk, Belarus

A. A. Valente · J. Rocha
Department of Chemistry, CICECO, University of Aveiro,
3810-193 Aveiro, Portugal

Present address: V. V. Kharton
Department of Ceramics and Glass Engineering, CICECO,
University of Aveiro, 3810-193 Aveiro, Portugal

Introduction

Oxide phases with mixed oxygen ionic and electronic conductivity are of great interest as materials of dense ceramic membranes for oxygen separation from air and partial oxidation of light hydrocarbons, in particular, for the conversion of CH_4 to synthesis gas [1, 2, 3, 4, 5]. Conventional technologies for natural gas conversion are based on steam reforming, which is energy intensive due to the highly endothermic nature of the reaction, and/or on partial oxidation, which requires significant capital investments for an oxygen plant. In contrast, membrane electrocatalytic reactors combine oxygen separation, partial oxidation and reforming in one single step [3, 4, 5, 6]. The ceramic membrane materials should satisfy a number of requirements, including high oxygen semipermeability and chemical and dimensional stability in a wide range of oxygen pressures and temperatures.

One promising group of mixed conductors is $La_{0.3}Sr_{0.7}(Fe,Ga)O_{3-\delta}$, having an ABO_3 perovskite lattice under oxidizing conditions and a brownmillerite-like vacancy-ordered structure at low $p(O_2)$ [6, 7, 8, 9]. Substitution of iron for gallium, the maximum solid solubility of which is about 30% [8], suppresses thermal and chemical expansion due to decreasing oxygen nonstoichiometry variations under changing oxygen pressure or temperature [6, 9]. Also, statistical distribution of

the B site cations may partially prevent oxygen vacancy ordering, probably due to local lattice distortions near Ga ions [7]. This leads to increasing ionic conduction below 1123 K, whilst at higher temperatures ionic transport decreases with Ga additions [8]. The oxygen permeation fluxes through $La_{0.3}Sr_{0.7}(Fe,Ga)O_{3-\delta}$ membranes [8] are 10–20 times lower than those of Co-containing perovskites [10, 11, 12].

This work presents data on the ionic and electronic transport properties, Seebeck coefficient and thermal expansion of $La_{0.3}Sr_{0.7}Co_{0.8}Ga_{0.2}O_{3-\delta}$ ceramics, with particular emphasis on the behavior under an air/CH_4 gradient. The parent compound, perovskite-type cobaltite $La_{0.3}Sr_{0.7}CoO_{3-\delta}$, exhibits one of the highest levels of oxygen permeability known for mixed conducting oxides [5, 10, 11]. In fact, a higher oxygen permeation has been reported only for Bi_2O_3-based composite materials and several perovskite phases derived from $A(Co,Fe)O_{3-\delta}$ (A = Sr, Ba), which exhibit, however, poor mechanical properties and sinterability [1, 10, 12]. Since the reduction of cobalt(II) oxide occurs at moderate oxygen chemical potentials [13], the stability of Co-containing materials may be insufficient for the use in electrocatalytic reactors. Special attention was therefore focused on the estimation of phase stability boundaries of $La_{0.3}Sr_{0.7}Co_{0.8}Ga_{0.2}O_{3-\delta}$. Since very reasonable results on $La_2Ni_{0.9}Co_{0.1}O_{4+\delta}$ stability limits were previously obtained from the data on total conductivity and Seebeck coefficient as functions of the oxygen partial pressure [14], a similar technique was used in this work. One should also note that, during the membrane operation, the oxygen chemical potential at the surface of membrane permeate side should be higher than that in the gas phase, particularly in the case of significant surface limitations to oxygen transport, characteristic of $La_{0.3}Sr_{0.7}CoO_{3-\delta}$ [11]. This makes it possible to expect kinetic stabilization of $La_{0.3}Sr_{0.7}CoO_3$-based ceramics under large oxygen chemical potential gradients, as for $La_2Ni_{0.9}Co_{0.1}O_{4+\delta}$ [14].

Experimental

The submicron powder of perovskite-type $La_{0.3}Sr_{0.7}Co_{0.8}Ga_{0.2}O_{3-\delta}$ was synthesized via the glycine–nitrate process (GNP), a self-combustion technique using glycine as fuel and nitrates of the metal components as oxidant [15]. Glycine was added to an aqueous solution, containing metal nitrates in the stoichiometric proportion (glycine/nitrate molar ratio of 2.0). After drying and combustion, the powder was fired in air at 1073 K for 2 h. The disc-shaped samples (12–15 mm in diameter) were uniaxially pressed at 250–350 MPa; sintering of dense ceramics was performed in air at 1533–1553 K for 2 h with subsequent slow cooling, in order to equilibrate with atmospheric oxygen at low temperatures. The formation of a single cubic perovskite phase was verified by X-ray diffraction (XRD) analysis. The density of $La_{0.3}Sr_{0.7}Co_{0.8}Ga_{0.2}O_{3-\delta}$ ceramics determined by the standard pyknometric technique, was 96.5 ±0.2% of the theoretical density calculated from XRD results (Table 1). The microstructural characterization was performed using transmission electron microscopy (TEM, Hitachi H-9000) and scanning electron microscopy (SEM, Hitachi S-4100), both combined with energy dispersive spectroscopy (EDS). Dilatometric data were collected in air using an alumina Linseis L70/2001 dilatometer (heating rate of 5 K/min). The total conductivity (four-probe DC) and Seebeck coefficient were measured at 300–1270 K in the oxygen partial pressure range from 60 kPa down to 2×10^{-13} Pa, as described elsewhere [7, 14]. The measurements of steady-state oxygen permeation fluxes through gas-tight ceramic membranes were carried out at 1023–1223 K; a detailed description of the experimental technique has been published earlier [8, 10]. For all permeation data presented in this paper, the feed-side oxygen partial pressure (p_2) was fixed at 21 kPa (atmospheric air).

The studies of dry methane oxidation were performed at 1123–1223 K with a set-up comprising one dense $La_{0.3}Sr_{0.7}Co_{0.8}Ga_{0.2}O_{3-\delta}$ membrane, hermetically sealed onto a 8% yttria-stabilized zirconia (Y8SZ) tube, and one electrochemical oxygen sensor at the outlet. The membrane feed side was exposed to atmospheric air. High-purity (≥99.995%) CH_4diluted with He (50:50 vol%) was supplied onto the membrane permeate side (effective surface area of 0.6 cm^2); the gas composition and flow rate at the inlet were fixed by Bronkhorst mass-flow controllers. As the role of surface processes

Table 1 Properties of perovskite oxide ceramics

Composition	Relative density[a] d_{exp}/d_{theor} (%)	Unit cell parameter a(nm)	Thermal expansion coefficients in air		Activation energy for total conductivity in air	
			T(K)	$\tilde{\alpha}\times10^6(K^{-1})$	T(K)	E_a (kJ/mol)
$La_{0.3}Sr_{0.7}Co_{0.8}Ga_{0.2}O_{3-\delta}$	96.5	0.3871	360–710 710–1030	15.9 ± 0.5 27.9 ± 0.4	300–800	8.1 ± 0.4
$La_{0.3}Sr_{0.7}Fe_{0.8}Ga_{0.2}O_{3-\delta}$	92.7	0.3883	300–920 920–1110	12.9 ± 0.3 25 ± 1	300–800	16.6 ± 0.4
$La_{0.3}Sr_{0.7}CoO_{3-\delta}$	92.6	0.3836	300–750 750–1100	19.6 ± 0.5 28.8 ± 0.5	410–685	2.7 ± 0.6

[a]Note: d_{exp} and d_{theor} are the experimental and theoretical densities, respectively

may become critical in reducing atmospheres [16, 17], catalytically active porous Pt layers with a sheet density of 8.6 mg cm^{-2} were applied onto the permeate-side surface. The gas flow rate at the reactor outlet, measured by a soap-film flowmeter, varied in the range 2.1–6.6 cm^3/min. The influent and effluent gas mixtures were analyzed using a Varian CP-3800 gas chromatograph, equipped with thermal conductivity and flame ionization detectors coupled in series and a 250 μL six-port VICI gas-sampling valve. The separation and quantification of the gas components was accomplished with a semi-capillary CarboPLOT P7 column using the absolute calibration method. No impurities in the initial gas mixture and no leaking of air into the cell were observed. The carbon imbalance between the inlet and outlet gas flows, monitored in the course of experiments, was within the limits of experimental uncertainty ($\pm 5\%$). The reaction selectivity was calculated as the concentration ratio between a given product and the sum of all detected C-containing products, namely CO, CO_2, C_2H_6, C_2H_4 and C_2H_2.

Results and discussion

General characterization

TEM and electron diffraction inspections (Fig. 1A) showed that $La_{0.3}Sr_{0.7}Co_{0.8}Ga_{0.2}O_{3-\delta}$ powder annealed at 1073 K consists of submicron-size particles, probably not completely crystallized. A single phase having cubic perovskite-type structure is formed during the sintering of ceramics; one example of XRD pattern is given in Fig. 2. Table 1 compares the unit cell parameter of $La_{0.3}Sr_{0.7}Co_{0.8}Ga_{0.2}O_{3-\delta}$ with those of $La_{0.3}Sr_{0.7}Fe_{0.8}Ga_{0.2}O_{3-\delta}$ and $La_{0.3}Sr_{0.7}CoO_{3-\delta}$ perovskites [8, 11]. As for the $La_{0.3}Sr_{0.7}(Fe,Ga)O_{3-\delta}$ system [8], doping of $La_{0.3}Sr_{0.7}CoO_{3-\delta}$ with gallium results in increasing unit cell volume. Taking into account that the radius of six-coordinated Ga^{3+} is smaller than those of high-spin Co^{3+} and Fe^{3+}, but larger than those of Co^{4+} and Fe^{4+} cations [18], this behavior can be attributed to the presence of a large fraction of tetravalent cobalt or iron and/or to an increasing level of structural disorder induced by Ga doping [7, 8]. The latter hypothesis was confirmed by data on the oxygen thermodynamics of $La_{0.3}Sr_{0.7}(Fe,Ga)O_{3-\delta}$ [7].

The sintering behavior of green compacts, made of GNP-synthesized powders of $La_{0.3}Sr_{0.7}M_{0.8}Ga_{0.2}O_{3-\delta}$ (M = Co, Fe), is compared in Fig. 3. As expected, both submicron powders demonstrate an enhanced sintering ability. The densification starts already at 1000–1100 K, with maximum shrinkage at 1170–1180 K. However, the materials with sufficiently high density (Table 1) can be sintered only at 1533–1553 K. Figure 1B shows SEM micrographs reflecting the microstructure characteristic of $La_{0.3}Sr_{0.7}Co_{0.8}Ga_{0.2}O_{3-\delta}$ ceramics. The grain size is 30 to 70 μm. Minor traces of a glassy phase are observed at the grain boundaries, indicating a liquid phase-assisted sintering process. Notice, however, that no deviations from the formula cation composition were detected by EDS.

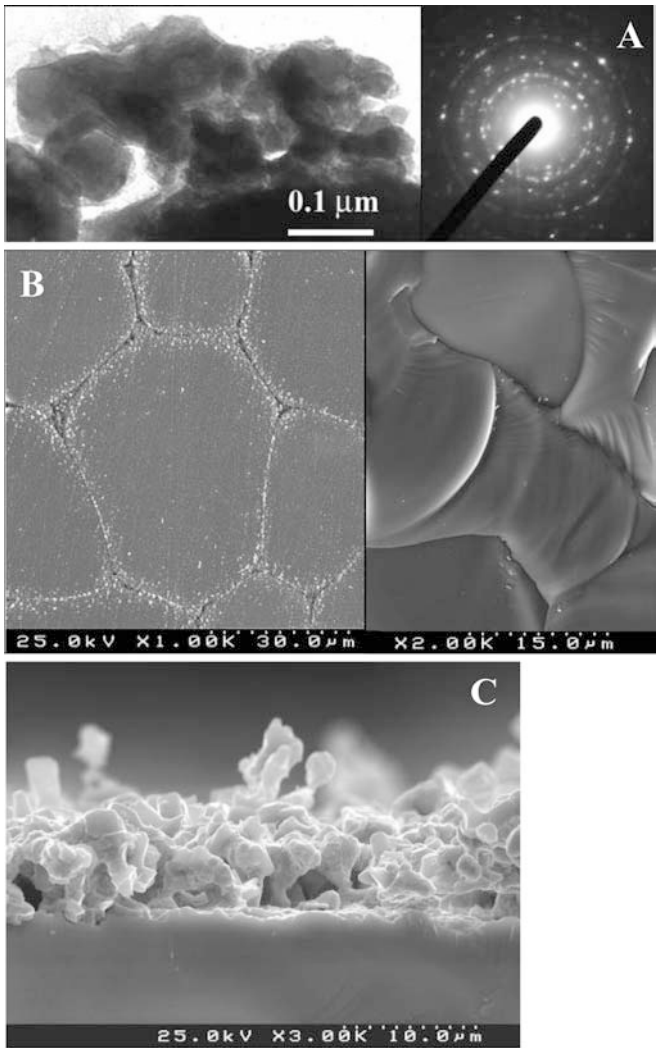

Fig. 1 **A** Bright-field TEM image (*left*) and electron diffraction pattern (*right*) of $La_{0.3}Sr_{0.7}Co_{0.8}Ga_{0.2}O_{3-\delta}$ synthesized by GNP and annealed at 1073 K for 2 h. **B** SEM micrographs of $La_{0.3}Sr_{0.7}Co_{0.8}Ga_{0.2}O_{3-\delta}$ ceramics, polished and thermally etched (*left*) and fractured (*right*). **C** SEM micrograph of a membrane cross-section with porous Pt layer on the permeate side, after the operation under an air/CH_4 gradient at 1123–1223 K

Dilatometric curves of $La_{0.3}Sr_{0.7}Co_{0.8}Ga_{0.2}O_{3-\delta}$ ceramics (Fig. 4) exhibit a break at 700–750 K, typical for most perovskites containing cobalt or iron [9, 12, 19]. The apparent increase of thermal expansion on heating is associated with progressive oxygen losses, which cause additional lattice expansion due to the decreasing oxidation state of B-site cations and the corresponding increase in their radii [9]. Also, a significant contribution due to progressive disordering in the oxygen sublattice on heating can be expected [9]. The average thermal expansion coefficients (TECs) of $La_{0.3}Sr_{0.7}Co_{0.8}Ga_{0.2}O_{3-\delta}$ are 15.9×10^{-6} and 27.9×10^{-6} K^{-1} in the low- and high-temperature ranges, respectively

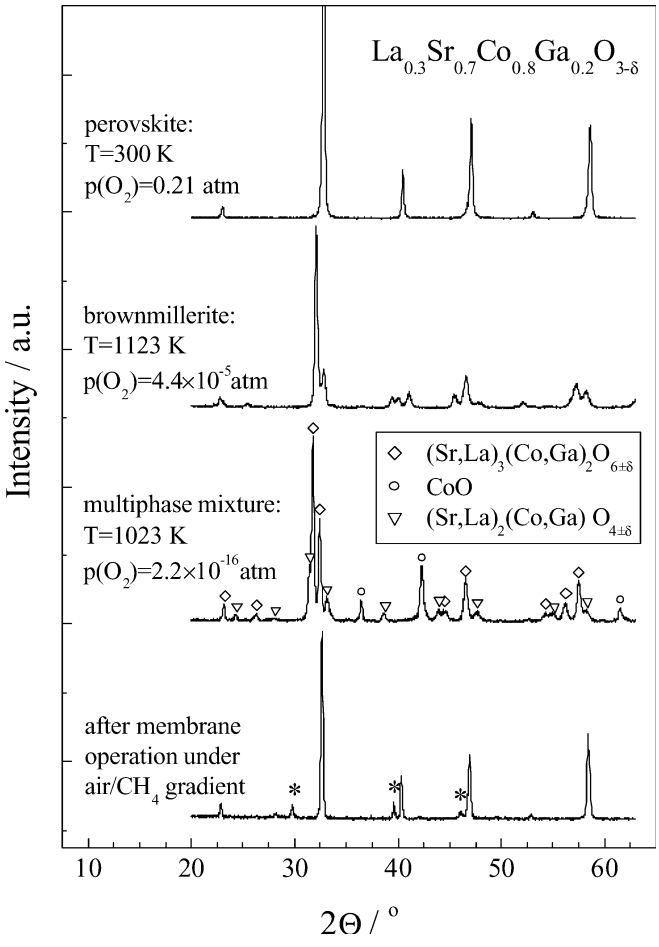

Fig. 2 XRD patterns of $La_{0.3}Sr_{0.7}Co_{0.8}Ga_{0.2}O_{3-\delta}$ ceramics after sintering in air at 1533 K for 2 h (*top*), after annealing at reduced oxygen pressures corresponding to different phase domains, with subsequent quenching (*center*), and after the membrane operation under an air/CH_4 gradient (permeate-side surface, *bottom*)

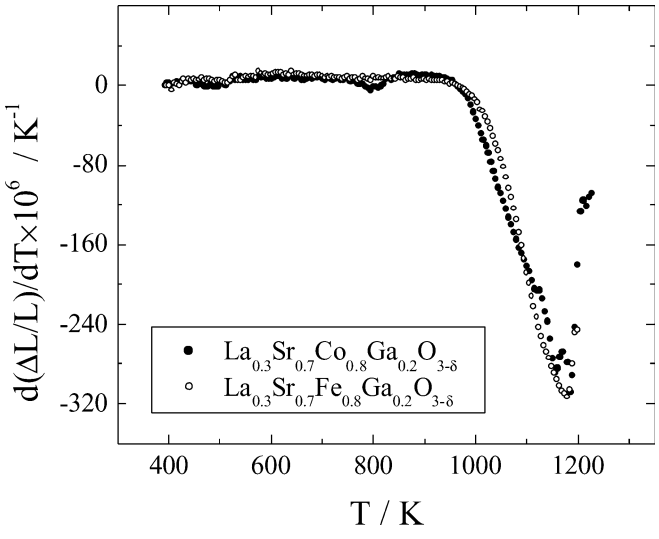

Fig. 3 Relative shrinkage of $La_{0.3}Sr_{0.7}Co_{0.8}Ga_{0.2}O_{3-\delta}$ and $La_{0.3}Sr_{0.7}Fe_{0.8}Ga_{0.2}O_{3-\delta}$ green compacts

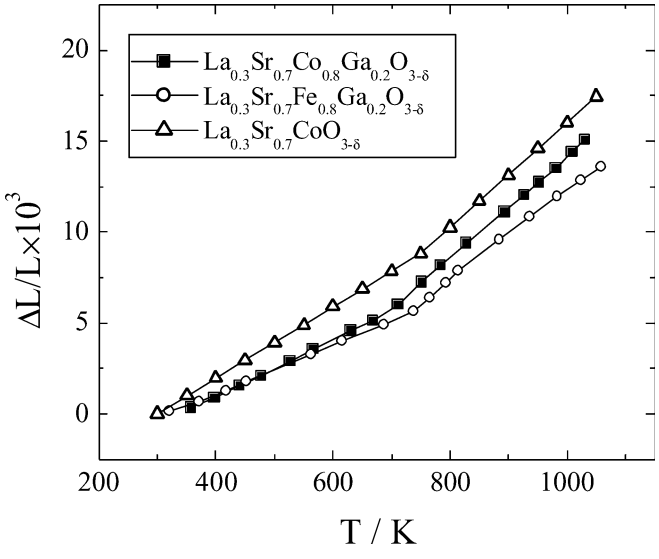

Fig. 4 Dilatometric curves of $La_{0.3}Sr_{0.7}Co_{0.8}Ga_{0.2}O_{3-\delta}$, $La_{0.3}Sr_{0.7}Fe_{0.8}Ga_{0.2}O_{3-\delta}$ and $La_{0.3}Sr_{0.7}CoO_{3-\delta}$ ceramics in air

(Table 1). As expected, these values are lower than those of $La_{0.3}Sr_{0.7}CoO_{3-\delta}$. Therefore, similar to the (La,Sr)(Fe,Ga)$O_{3-\delta}$ system [8, 9], doping with gallium suppresses thermal expansion of lanthanum–strontium cobaltites. In the case of $La_{0.3}Sr_{0.7}Co_{0.8}Ga_{0.2}O_{3-\delta}$, however, such a decrease is insufficient; the high-temperature TEC of this material is incompatible with the thermal expansion of common construction materials, such as alumina, zirconia or stainless steels. The use of $La_{0.3}Sr_{0.7}Co_{0.8}Ga_{0.2}O_{3-\delta}$ ceramics is hence possible only in tubular reactors, with hermetization in a low-temperature zone.

Phase stability

Typical examples of the oxygen partial pressure dependencies of total conductivity (σ) and Seebeck coefficient (α) of $La_{0.3}Sr_{0.7}Co_{0.8}Ga_{0.2}O_{3-\delta}$ are presented in Fig. 5. The behavior of electrical properties suggests the presence of at least four distinct phase domains ascertained by XRD. For oxygen pressures greater than approximately 7–10 Pa (domain I), decreasing $p(O_2)$ leads to a significant increase in thermopower and a decrease in conductivity, both indicating dominant pseudometallic electron–hole transport. Domain II corresponds to a plateau-like behavior at oxygen pressures below 5–7 Pa. The low-$p(O_2)$ boundary of this domain varies from 8×10^{-10} up to 3×10^{-4} Pa when the temperature increases in the range 973–1223 K. For domain II, the electrical properties are almost independent of $p(O_2)$, keeping the tendencies characteristic of a pseudometallic p-type conduction. According to the XRD data (Fig. 2), domains I and II correspond to the perovskite- and brownmillerite-type polymorphs of $La_{0.3}Sr_{0.7}$

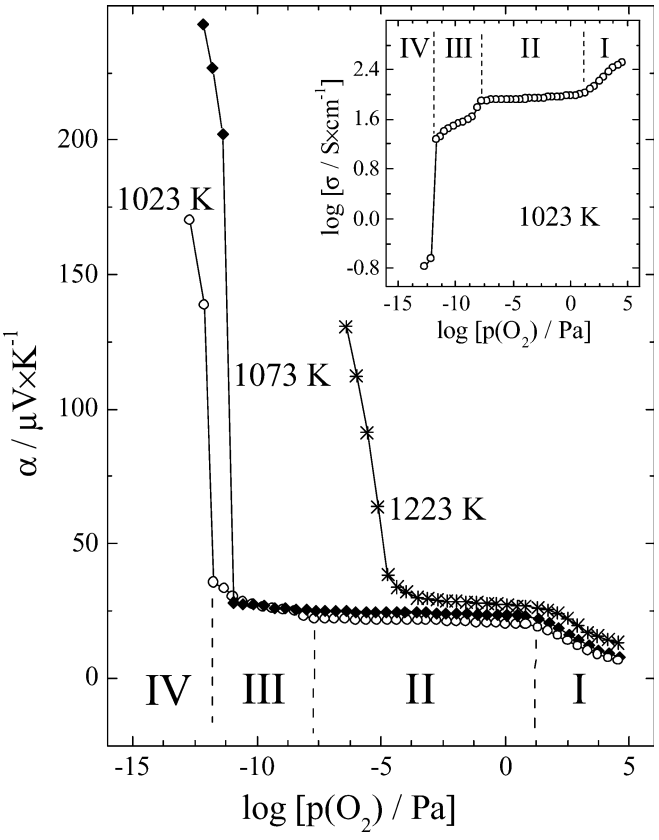

Fig. 5 Examples of the oxygen partial pressure dependencies of the Seebeck coefficient of $La_{0.3}Sr_{0.7}Co_{0.8}Ga_{0.2}O_{3-\delta}$. Inset shows $p(O_2)$ dependence of the total conductivity at 1023 K. Dashed lines indicate approximate phase boundaries at 1023 K (see text)

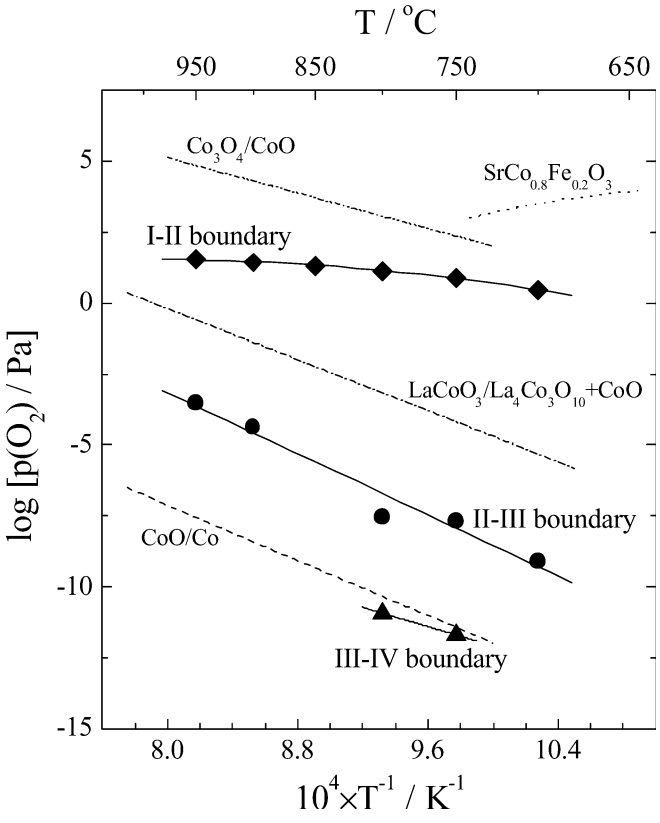

Fig. 6 Approximate phase stability boundaries of $La_{0.3}Sr_{0.7}Co_{0.8}Ga_{0.2}O_{3-\delta}$, evaluated from the data on total conductivity and Seebeck coefficient as functions of $p(O_2)$. Literature data on Co_3O_4 [13], CoO [13], $LaCoO_{3-\delta}$ [21], and $SrCo_{0.8}Fe_{0.2}O_{3-\delta}$ [22] are shown for comparison

$Co_{0.8}Ga_{0.2}O_{3-\delta}$; the latter phase is isostructural with $Sr_2Co_2O_5$(PDF card 34-1475). Further reduction leads to the formation of multiphase mixtures consisting of $(Sr,La)_3(Co,Ga)_2O_6$- and $(La,Sr)_2(Co,Ga)O_4$-based solid solutions and CoO; this is accompanied by a moderate decrease in conductivity (domain III). Finally, at oxygen pressures close to the Co/CoO boundary (Fig. 6), the oxide phase mixture is reduced to metallic cobalt and binary metal oxides, which results in a dramatic conductivity drop (domain IV in Fig. 5). Based on the XRD analysis of $La_{0.3}Sr_{0.7}Co_{0.8}Ga_{0.2}O_{3-\delta}$ samples quenched after annealing at various $p(O_2)$, such a decomposition mechanism is quite similar to that reported for $La_{0.3}Sr_{0.7}CoO_{3-\delta}$ at 1373 K [20].

Figure 6 compares phase boundaries of $La_{0.3}Sr_{0.7}Co_{0.8}Ga_{0.2}O_{3-\delta}$ with the stability limits of binary cobalt oxides [13], and perovskite-type $LaCoO_{3-\delta}$ [21] and $SrCo_{0.8}Fe_{0.2}O_{3-\delta}$ [22]. The transition "perovskite↔brownmillerite" of the title compound occurs at oxygen partial pressures 10^2–10^4 times lower than the decomposition limits of Co_3O_4 and $SrCo_{0.8}Fe_{0.2}O_{3-\delta}$, but about 10^3 times higher than that of lanthanum cobaltite. The unusual behavior of $SrCo_{0.8}Fe_{0.2}O_{3-\delta}$ is associated with a complex reduction mechanism; in moderately reducing atmospheres $Sr(Co,Fe)O_{3-\delta}$ perovskites transform into brownmillerite-type $Sr_2(Co,Fe)_2O_5$at temperatures above 900–1100 K and to a mixture of hexagonal $Sr_6(Co,Fe)_5O_{15}$ and Co_3O_4 at low temperatures (refs. [22, 23] and references cited therein). If compared to the reduction of $LaCoO_{3-\delta}$ yielding $La_4Co_3O_{10}$ and CoO [21], the decomposition of the brownmillerite modification of $La_{0.3}Sr_{0.7}Co_{0.8}Ga_{0.2}O_{2.5\pm\delta}$ occurs at lower $p(O_2)$, but is characterized by a similar enthalpy. It is noteworthy that, in the case of $La_{0.3}Sr_{0.7}(Fe,Ga)O_{3-\delta}$, the transition from disordered perovskite to the brownmillerite-like modifications has no essential effect on the oxygen ionic conductivity [8].

Figure 7 shows the relationships between typical $p(O_2)$ values in the membrane reactor effluent gas mixtures, calculated from the electrochemical sensor e.m.f., and the low $p(O_2)$ stability limit of brownmillerite-like $La_{0.3}Sr_{0.7}Co_{0.8}Ga_{0.2}O_{2.5\pm\delta}$ (II–III boundary in Fig. 6). Under equilibrium conditions, the membrane should be completely decomposed in the flow of methane oxidation products. However, XRD analysis of the membrane permeate-side surface after the operation at 1123–1223 K shows that the perovskite phase is still dominant (Fig. 2, bottom). Only minor peaks of Pt catalyst and La_2O_3, marked by asterisks in the XRD pattern, were observed in addition to the major perovskite reflections; the formation of lanthanum oxide is caused, most likely,

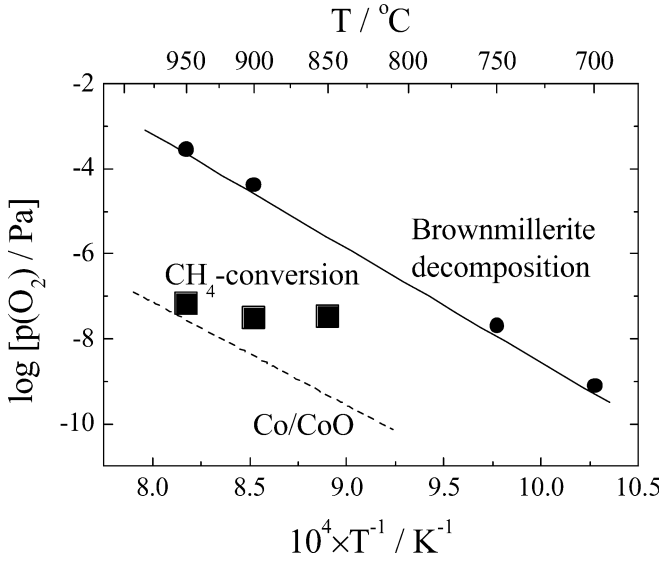

Fig. 7 Comparison of typical $p(O_2)$ values in the membrane reactor effluent gas and the low-$p(O_2)$ stability limit of brownmillerite-like $La_{0.3}Sr_{0.7}Co_{0.8}Ga_{0.2}O_{2.5\pm\delta}$

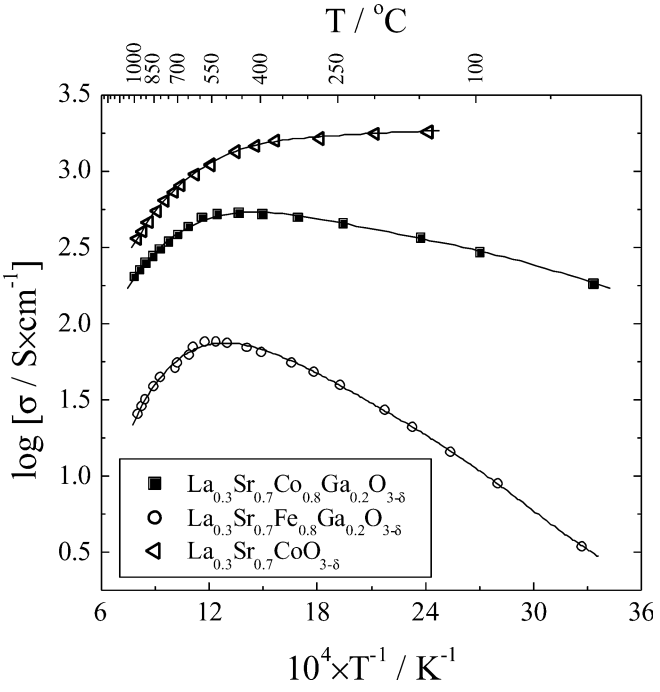

Fig. 8 Temperature dependence of total conductivity of $La_{0.3}Sr_{0.7}Co_{0.8}Ga_{0.2}O_{3-\delta}$, $La_{0.3}Sr_{0.7}Fe_{0.8}Ga_{0.2}O_{3-\delta}$ and $La_{0.3}Sr_{0.7}CoO_{3-\delta}$, in air

by cation demixing under an oxygen chemical potential gradient [5]. This behavior suggests that, as for $La_2Ni_{0.9}Co_{0.1}O_{4+\delta}$ membranes [14], kinetic stabilization of $La_{0.3}Sr_{0.7}Co_{0.8}Ga_{0.2}O_{3-\delta}$ under non-equilibrium conditions takes place, probably due to surface-limited oxygen transport.

p-Type electronic transport in $La_{0.3}Sr_{0.7}Co_{0.8}Ga_{0.2}O_{3-\delta}$ perovskite

The temperature dependence of total conductivity of $La_{0.3}Sr_{0.7}Co_{0.8}Ga_{0.2}O_{3-\delta}$ in air exhibits a pseudometallic character at temperatures above 750 K (Fig. 8). Similar trends in behavior are characteristic of $La_{0.3}Sr_{0.7}Fe_{0.8}Ga_{0.2}O_{3-\delta}$ and $La_{0.3}Sr_{0.7}CoO_{3-\delta}$. If compared to the latter, the conductivity of $La_{0.3}Sr_{0.7}Co_{0.8}Ga_{0.2}O_{3-\delta}$ is lower since the substitution of cobalt for gallium, having a constant oxidation state, decreases the concentration of the B sites contributing to the electron–hole conduction. As for $La_{0.3}Sr_{0.7}(Fe,Ga)O_{3-\delta}$ [7, 8], Ga doping leads not only to lower charge carrier concentration, but also to decreasing hole mobility provided by the Co–O–Co bonds [24], a part of which is blocked by gallium cations. This is reflected by the higher activation energy (E_a) for the total conductivity of $La_{0.3}Sr_{0.7}Co_{0.8}Ga_{0.2}O_{3-\delta}$ than that of $La_{0.3}Sr_{0.7}CoO_{3-\delta}$ in the low-temperature range (Table 1).

As mentioned above, the oxygen pressure dependencies of total conductivity and Seebeck coefficient of $La_{0.3}Sr_{0.7}Co_{0.8}Ga_{0.2}O_{3-\delta}$ perovskite (Fig. 9) clearly show that the p-type electronic transport is predominant. All these curves are non-linear, with a maximum slope at moderate oxygen partial pressures varying from 0.1 to 2 kPa. In this $p(O_2)$ range, the exponent of σ versus $p(O_2)^{1/m}$dependencies (Table 2) is close to 1/6, a classical value for a mixed conductor with moderate oxygen nonstoichiometry [25]. The conclusion that the p-type conduction is dominant, is in agreement with oxygen permeation data discussed below. Although the calculation of exact values of the oxygen ionic conductivity is impossible due to a significant interfacial effect on the oxygen permeation, the estimates of the ionic contribution to total conductivity are less than 0.2%.

For the Seebeck coefficient, the slope of α versus ln $p(O_2)$ is, however, considerably lower than $(-k/6e)$, which could be expected in the case of a simple band mechanism of the hole conduction. This may suggest a hopping mechanism with $p(O_2)$-dependent mobility. In this case, neglecting the transported heat of the holes and possible blocking effects, the Seebeck coefficient can be expressed as [25, 26, 27]

$$\alpha = \frac{k}{e}\ln\left(\frac{N-[h]}{[h]}\right) \quad (1)$$

where [h] is the hole concentration, and N is the concentration of sites participating in the conduction process. Both the hole mobility, defined as $\mu=(\sigma/e[h])$, and the values of N may be affected by the oxygen chemical potential. Such a situation may take place, for example, if a part of cobalt sites is blocked due to an association with oxygen vacancies, characteristic of $(La,Sr)CoO_{3-\delta}$ [5]. The estimations of the $[h]/N$ ratio using Eq. (1) give quite reasonable values, decreasing when the temperature increases or the oxygen partial pressure decreases.

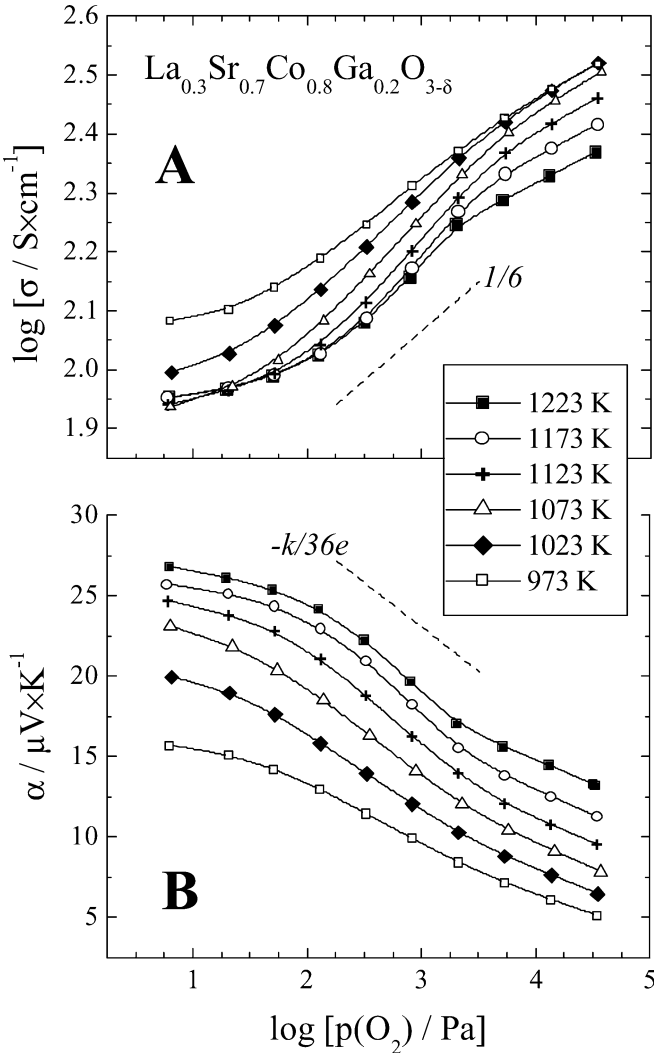

Fig. 9 Oxygen partial pressure dependencies of the total conductivity (**A**) and Seebeck coefficient (**B**) of $La_{0.3}Sr_{0.7}Co_{0.8}Ga_{0.2}O_{3-\delta}$ under oxidizing conditions. Solid lines are for visual guidance only

Table 2 Slope parameter (m) of the $p(O_2)$ dependencies of total conductivity[a] of $La_{0.3}Sr_{0.7}Co_{0.8}Ga_{0.2}O_{3-\delta}$

T(K)	Oxygen partial pressure range	
	0.1–2 kPa	2–30 kPa
973	6.6 ± 0.5	8 ± 1
1023	5.4 ± 0.2	7.5 ± 1
1073	4.9 ± 0.2	7 ± 2
1123	4.8 ± 0.8	7 ± 3
1173	5 ± 1	8 ± 3
1223	5 ± 2	9.9 ± 0.1

[a]The model for conductivity: $\sigma = \sigma_p{}^0 p(O_2)^{1/m}$, where m and $\sigma_p{}^0$ are constants

This makes it possible to calculate (μN), although the mobility cannot be extracted without the knowledge of the exact transport mechanism.

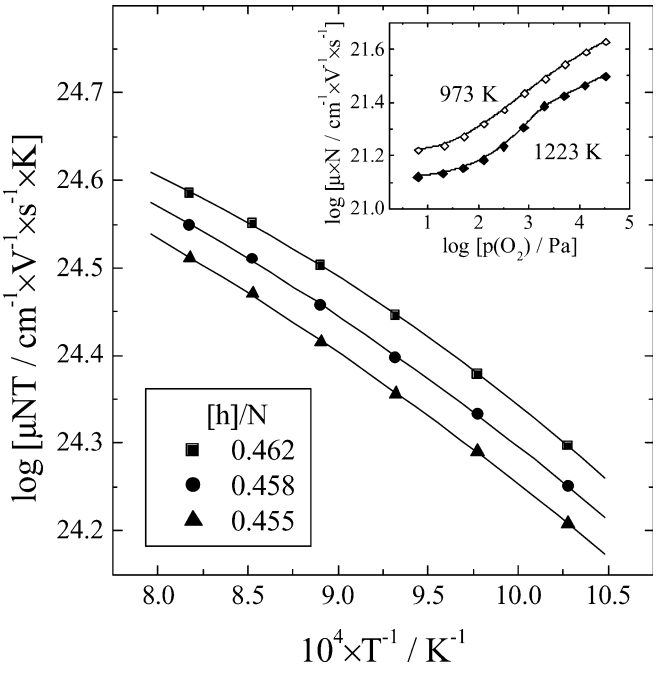

Fig. 10 Arrhenius plots of the μN product, calculated from the total conductivity and Seebeck coefficient of $La_{0.3}Sr_{0.7}Co_{0.8}Ga_{0.2}O_{3-\delta}$ perovskite phase, at fixed p/N ratios (see text). Inset shows the oxygen partial pressure dependencies of μN

Figure 10 presents Arrhenius plots of the μN product at fixed [h]/N ratios. The hole mobility has a temperature-activated character typical for the small-polaron mechanism [26]. In other words, at a fixed hole concentration the conductivity is semiconductor like. Therefore, as for $La_2Ni_{0.9}Co_{0.1}O_{4+\delta}$ [14], the pseudo-metallic behavior of $La_{0.3}Sr_{0.7}Co_{0.8}Ga_{0.2}O_{3-\delta}$ (Fig. 8) is due to oxygen losses on heating.

One should also note that the increase in hole mobility with increasing oxygen pressure (inset in Fig. 10) is often observed in perovskite-related phases, such as ferrites and cuprates [7, 28]. As mentioned above, this may be attributed to progressive association of oxygen vacancies and Co^{2+} ions on reducing $p(O_2)$, decreasing concentration of the cobalt sites available for hole hopping. Another possible explanation refers to the perovskite unit cell contraction when the oxygen non-stoichiometry decreases and the average oxidation state of cobalt cations increases [7]. This leads to a greater overlap of cobalt and oxygen electron orbitals and, thus, to a stronger covalency of Co–O–Co bonds, providing higher mobility [24].

Surface-limited oxygen transport

Selected results on the oxygen permeation through $La_{0.3}Sr_{0.7}Co_{0.8}Ga_{0.2}O_{3-\delta}$ membranes with various thickness are presented in Fig. 11A. The values of the specific oxygen permeability $J(O_2)$, given in Fig. 11B, are related to the permeation flux density j as [8, 10, 11]

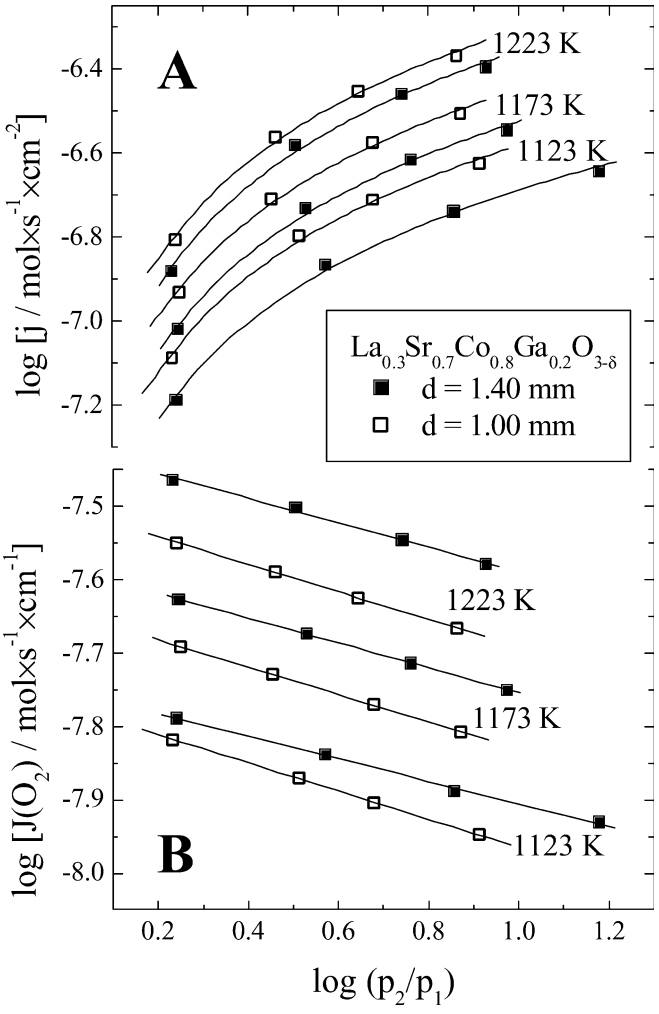

Fig. 11 Dependence of the oxygen permeation fluxes (**A**) and specific oxygen permeability (**B**) of $La_{0.3}Sr_{0.7}Co_{0.8}Ga_{0.2}O_{3-\delta}$ membranes on the oxygen partial pressure gradient

$$j = \frac{J(O_2)}{d} \ln\left(\frac{p_2}{p_1}\right) \quad (2)$$

where d is the membrane thickness, p_1 and p_2 are the oxygen partial pressures at the membrane permeate and feed sides, respectively. Since the quantity $J(O_2)$ is, by definition, proportional to jd, the specific permeability would be independent of thickness in the case of negligible effect of the processes at the membrane/gas boundaries. However, the data on $La_{0.3}Sr_{0.7}Co_{0.8}Ga_{0.2}O_{3-\delta}$ membranes unambiguously indicate that oxygen transport is determined by both bulk ambipolar conduction and oxygen surface exchange. The permeation fluxes decrease with increasing d, while $J(O_2)$ increases due to a decreasing role of the exchange rate. Similar behavior was earlier observed for $La_{0.3}Sr_{0.7}CoO_{3-\delta}$ and $La_{0.3}Sr_{0.7}FeO_{3-\delta}$ membranes [8, 11].

Further inspection of the permeation data (Fig. 11) suggests that the limiting effect of interfacial processes becomes greater when the temperature increases or the permeate-side oxygen pressure decreases. This is in excellent agreement with the isotopic exchange data on $La_{0.3}Sr_{0.7}CoO_{3-\delta}$ [29], which showed the activation energies for bulk oxygen diffusion and for the surface exchange to be equal to 56 and 28 kJ/mol, respectively. The oxygen diffusivity in $La_{0.3}Sr_{0.7}CoO_{3-\delta}$ was found to be independent of $p(O_2)$, whilst the interfacial exchange rate increases with oxygen pressure [29].

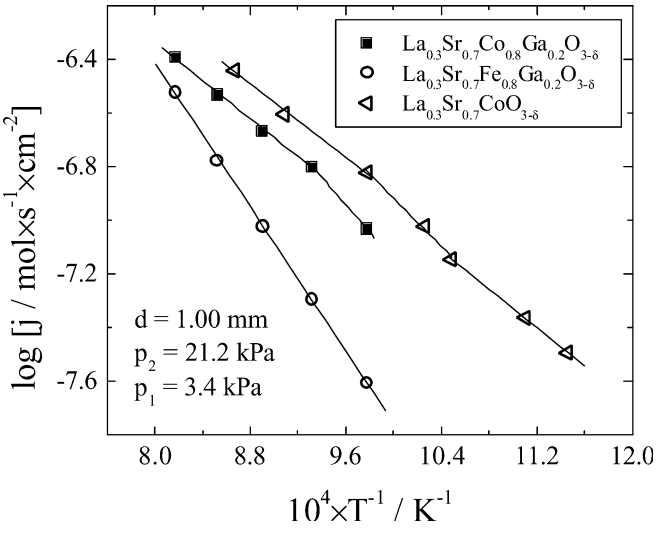

Fig. 12 Temperature dependence of the oxygen permeation fluxes through perovskite membranes under a fixed oxygen partial pressure gradient

Figure 12 compares the oxygen permeation fluxes through $La_{0.3}Sr_{0.7}Co_{0.8}Ga_{0.2}O_{3-\delta}$, $La_{0.3}Sr_{0.7}Fe_{0.8}Ga_{0.2}O_{3-\delta}$ and $La_{0.3}Sr_{0.7}CoO_{3-\delta}$ membranes under a fixed oxygen partial pressure gradient. As for other perovskite-type ferrites and cobaltites [1, 12, 30], the permeability of $La_{0.3}Sr_{0.7}Co_{0.8}Ga_{0.2}O_{3-\delta}$ is 1.5–4.0 times higher than that of the Fe-containing analogue. Doping of $La_{0.3}Sr_{0.7}CoO_{3-\delta}$ with gallium results in lower permeation fluxes, although the effective activation energies in both cobaltites are similar. Such a behavior can be explained by local lattice distortions near Ga ions, appearing due to significant difference in the covalency of Ga–O and Co–O chemical bonds [7, 8]. The distortions may favor trapping of the oxygen anions in the neighborhood of gallium cations, thus decreasing the concentration of mobile oxygen ions and, consequently, oxygen ionic conductivity, the latter being one of the permeation-determining factors. In the case of $La_{0.3}Sr_{0.7}(Fe,Ga)O_{3-\delta}$, the local lattice distortions near statistically distributed Ga^{3+} suppress long-range ordering in the oxygen sublattice, which leads to a higher ionic transport at temperatures below 1150–1200 K [8]. For $La_{0.3}Sr_{0.7}CoO_{3-\delta}$, however, the order–disorder transition appears at considerably lower temperatures, 950–1050 K [5, 31]; this transition is reflected as a break in the Arrhenius curve of the oxygen permeability of $La_{0.3}Sr_{0.7}CoO_{3-\delta}$ (Fig. 12). Therefore, at 973–1223 K the replacement of cobalt with gallium decreases oxygen transport.

Methane oxidation on $La_{0.3}Sr_{0.7}Co_{0.8}Ga_{0.2}O_{3-\delta}$ ceramics

Representative data on dry methane oxidation in a model reactor with a planar $La_{0.3}Sr_{0.7}Co_{0.8}Ga_{0.2}O_{3-\delta}$ membrane are given in Figs. 13 and 14. Due to increasing oxygen permeation flux, the methane conversion increases with temperature. Increasing flow rate of the influent gas has the opposite effect, as expected from thermodynamics. A maximum conversion of ca. 57% is achieved at 1223 K. However, CH_4 oxidation on the surface of a Ga-substituted cobaltite membrane results in very low CO yields, far from the thermodynamic equilibrium values. In all cases, the CO selectivity varied in the range 1–6%, increasing when the methane flow rate or temperature increases.

The selectivity to C2 hydrocarbons (C_2H_6, C_2H_4 and C_2H_2) is 1–4%. Contrary to literature data [32] and thermodynamic expectations, the trace amounts of C_2H_2 detected in the product mixture increased with temperature (Fig. 13). The formation of C2 hydrocarbons results, most likely, from thermally induced dissociation reactions rather than from the oxidative dimerization of methane.

The observed behavior seems to be in agreement with the CCR (combustion and reforming reaction) mechanism of the catalytic partial oxidation of methane [33]. The CCR mechanism involves full oxidation of CH_4 to CO_2 and H_2O, with subsequent reforming of residual methane by carbon dioxide and steam. Since no traces of O_2 were detected in the effluent mixtures, all permeated oxygen is probably consumed in the first stage of the reaction system, i.e. full combustion. Subsequently, in a second stage, reforming occurs in the gas phase and may be stagnated. Such a conclusion is supported by the comparative data on $La_{0.3}Sr_{0.7}Co_{0.8}Ga_{0.2}O_{3-\delta}$ and $La_2Ni_{0.9}Co_{0.1}O_{4+\delta}$ membranes (Fig. 15). The latter, a mixed conductor with K_2NiF_4-type structure, is another promising candidate for membrane reactors [14]. The higher oxygen permeability of $La_{0.3}Sr_{0.7}Co_{0.8}Ga_{0.2}O_{3-\delta}$ (Fig. 15A) leads to a higher methane conversion, but lower CO selectivity as compared to $La_2Ni_{0.9}Co_{0.1}O_{4+\delta}$ membrane (Fig. 15B).

The SEM/EDS analysis of $La_{0.3}Sr_{0.7}Co_{0.8}Ga_{0.2}O_{3-\delta}$ ceramics after the operation under an air/methane gradient (Fig. 1C) revealed no traces of bulk degradation. Also, the XRD pattern of the membrane permeate-side surface after electrocatalytic experiments (Fig. 2, bottom) showed that the perovskite-type phase was not reduced. These data confirm kinetic stabilization of mixed-conducting membranes due to surface limitations to the oxygen transport, when the oxygen chemical

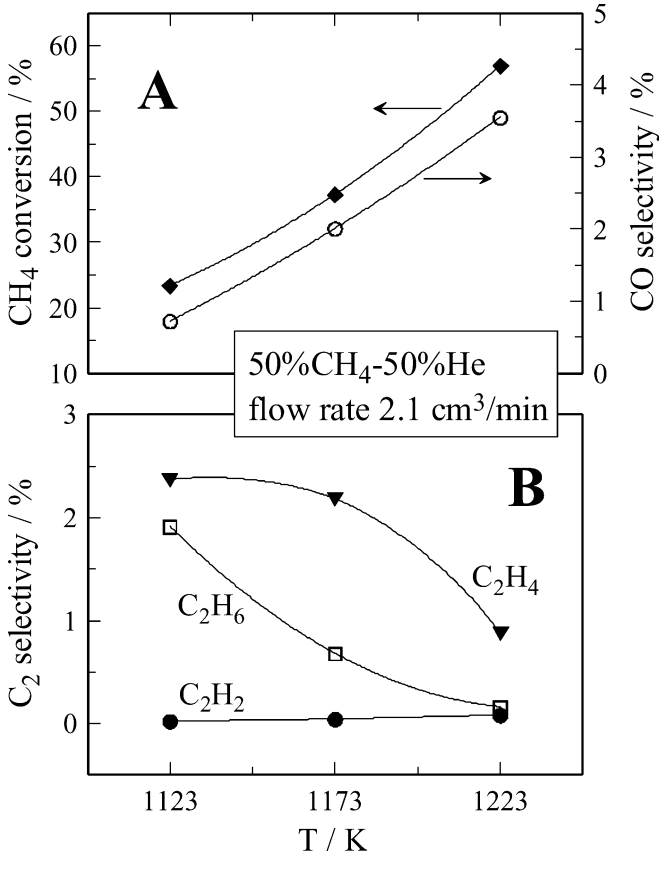

Fig. 13 Temperature dependencies of methane conversion efficiency and CO selectivity (**A**), and selectivities to C2 hydrocarbons (**B**) in a reactor with a $La_{0.3}Sr_{0.7}Co_{0.8}Ga_{0.2}O_{3-\delta}$ membrane ($d = 0.95$ mm, Pt layer)

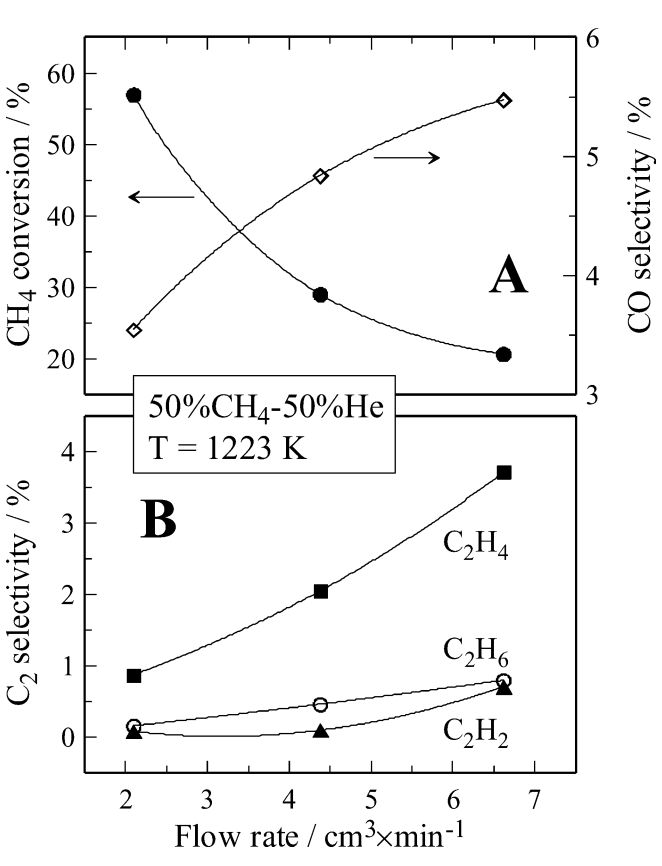

Fig. 14 Methane conversion and CO selectivity (**A**) and selectivities to C2 hydrocarbons (**B**) in a reactor with an $La_{0.3}Sr_{0.7}Co_{0.8}Ga_{0.2}O_{3-\delta}$ membrane ($d = 0.95$ mm, Pt layer) versus the influent gas flow rate

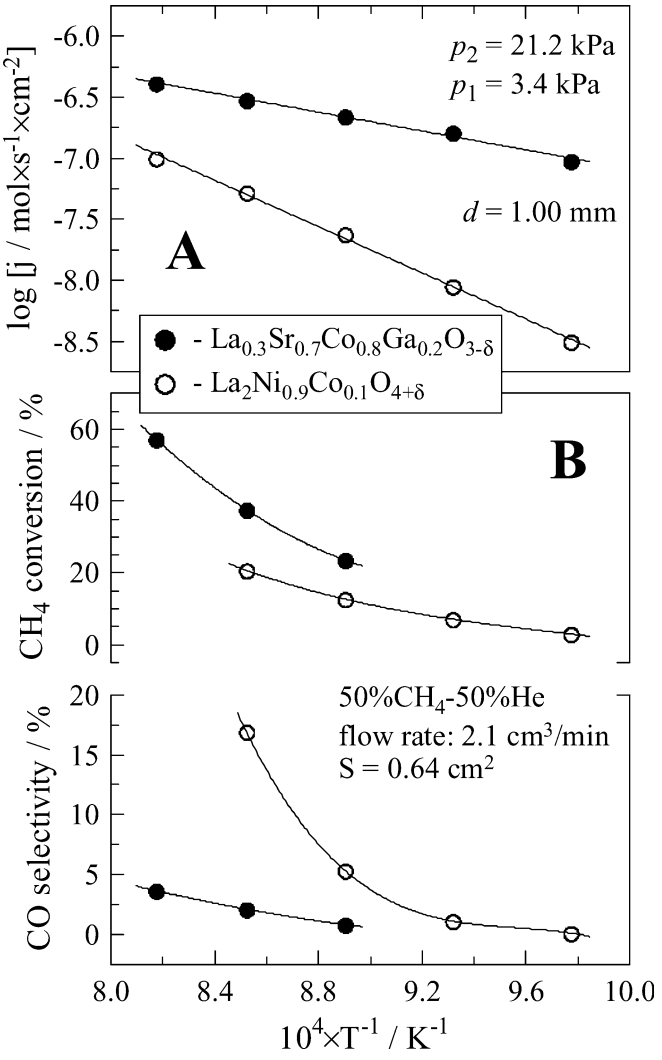

Fig. 15 Temperature dependencies of the oxygen permeation fluxes through $La_{0.3}Sr_{0.7}Co_{0.8}Ga_{0.2}O_{3-\delta}$ and $La_2Ni_{0.9}Co_{0.1}O_{4+\delta}$ membranes ($d = 1.00$ mm) under fixed oxygen partial pressure gradient (**A**), and the performance of $La_{0.3}Sr_{0.7}Co_{0.8}Ga_{0.2}O_{3-\delta}$ ($d = 0.95$ mm, Pt layer) and $La_2Ni_{0.9}Co_{0.1}O_{4+\delta}$ ($d = 0.60$ mm, Pt/$La_2Ni_{0.9}Co_{0.1}O_{4+\delta}$ layer) membranes for dry methane oxidation (**B**)

potential at the membrane surface is greater than that in the gas phase. In particular, the use of $La_{0.3}Sr_{0.7}Co_{0.8}Ga_{0.2}O_{3-\delta}$ ceramics for direct oxidation of dry methane is possible. However, the dominant mechanism of total CH_4 oxidation on the membrane/gas interface makes it necessary to incorporate a selective reforming catalyst in the reactor.

Conclusions

Single-phase $La_{0.3}Sr_{0.7}Co_{0.8}Ga_{0.2}O_{3-\delta}$ ceramics with 96.5% density were prepared by the glycine–nitrate technique and characterized by XRD, TEM, SEM/EDS, dilatometry and measurements of the total conductivity, Seebeck coefficient, oxygen permeability, and dry methane oxidation in model membrane reactors. The average thermal expansion coefficients in air are 15.9×10^{-6} and 27.9×10^{-6} K^{-1} at 360–710 and 710–1030 K, respectively. The total conductivity of $La_{0.3}Sr_{0.7}Co_{0.8}Ga_{0.2}O_{3-\delta}$ perovskite, which is predominantly p-type electronic and has an activation energy of 8.1 kJ/mol at 300–800 K in air, exhibits an apparent pseudometallic behavior due to oxygen losses on heating. The variations of electrical properties with oxygen pressure suggest a small-polaron conduction mechanism. Under equilibrium conditions, the reduction of the $La_{0.3}Sr_{0.7}Co_{0.8}Ga_{0.2}O_{3-\delta}$ perovskite phase occurs via several consecutive steps, including the transition into a brownmillerite-like phase at $p(O_2) = 4$–30 Pa, the decomposition into a multiphase oxide mixture at 8×10^{-10}–3×10^{-4} Pa, and further segregation of cobalt metal. Nevertheless, Ga-substituted cobaltite membranes are kinetically stable under an air/methane gradient due to significant surface limitations to the oxygen transport. The conversion of dry methane on $La_{0.3}Sr_{0.7}Co_{0.8}Ga_{0.2}O_{3-\delta}$ membranes increases with temperature and achieves 57% at 1223 K, whilst the low CO selectivity (< 6%) indicates a significant role of the complete CH_4 oxidation on the membrane surface. The total yield of C2 hydrocarbons in the product mixture at 1123–1223 K was lower than 6%.

Acknowledgements This work was partially supported by the NATO Science for Peace program (project 978002), the FCT, Portugal (POCTI program and Projects BD/6827/2001 and BPD/11606/2002), and the INTAS (project 00276). Experimental contributions made by A. Kovalevsky and N. Vyshatko are gratefully acknowledged.

References

1. Bouwmeester HJM, Burggraaf AJ (1996) Dense ceramic membranes for oxygen separation. In: Burggraaf AJ, Cot L (eds) Fundamentals of inorganic membrane science and technology. Elsevier, Amsterdam, pp 435–528
2. Kilner J, Benson S, Lane J, Waller D (1997) Chem Ind 17:907
3. Mazanec TJ (1994) Solid State Ionics 70/71:11
4. Dyer PN, Richards RE, Russek SL, Taylor DM (2000) Solid State Ionics 134:21
5. van Doorn RHE (1996) PhD Thesis. University of Twente, Enschede, Netherlands
6. Schwartz M, White JH, Sammells AF (2001) US Patent 6214757
7. Patrakeev MV, Mitberg EB, Lakhtin AA, Leonidov IA, Kozhevnikov VL, Kharton VV, Avdeev M, Marques FMB (2002) J Solid State Chem 167:203
8. Kharton VV, Yaremchenko AA, Viskup AP, Patrakeev MV, Leonidov IA, Kozhevnikov VL, Figueiredo FM, Shaulo AL, Naumovich EN, Marques FMB (2002) J Electrochem Soc 149:E125
9. Kharton VV, Yaremchenko AA, Patrakeev MV, Naumovich EN, Marques FMB (2003) J Eur Ceram Soc 23:1417
10. Kharton VV, Naumovich EN, Nikolaev AN (1996) J Membrane Sci 111:149
11. Kharton VV, Kovalevsky AV, Yaremchenko AA, Figueiredo FM, Naumovich EN, Shaulo AL, Marques FMB (2002) J Membrane Sci 195:277
12. Kharton VV, Yaremchenko AA, Naumovich EN (1999) J Solid State Electrochem 3:303

13. Tretiakov YuD (1974) Chemistry of nonstoichiometric oxides. Moscow State University, Moscow
14. Yaremchenko AA, Kharton VV, Patrakeev MV, Frade JR (2003) J Mater Chem 13:1136
15. Chick LA, Pederson LR, Maupin GD, Bates JL, Thomas LE, Exarhos GJ (1990) Mater Lett 10:6
16. ten Elshof JE, Bouwmeester HJM, Verweij H (1995) Appl Catal A 130:195
17. Xu SJ, Thomson WJ (1997) AIChE J 43:2731
18. Shannon RD (1976) Acta Crystallogr A32:751
19. Ullmann H, Trofimenko N, Tietz F, Stover D, Ahmad-Khanlou A (2000) Solid State Ionics 138:79
20. Cherepanov VA, Gavrilova LYa, Barkhatova LYu, Voronin VI, Trifonova MV, Bukhner OA (1998) Ionics 4:309
21. Petrov AN, Cherepanov VA, Zuev AYu (1987) Zh Fiz Khim 61:630
22. Tikhonovich VN, Naumovich EN, Logvinovich DI, Kharton VV, Vecher AA (2003) J Solid State Electrochem 7:77
23. Liu L-M, Lee TH, Qiu L, Yang YL, Jacobson AJ (1996) Mater Res Bull 31:29
24. Ramadass N (1978) Mater Sci Eng 36:231
25. Kofstad P (1972) Nonstoichiometry, diffusion and electrical conductivity in binary metal oxides. Wiley-Interscience, New York
26. Jonker GH (1968) Philips Res Rep 23:131
27. Kobayashi K, Yamaguchi S, Tsunoda T, Imai Y (2001) Solid State Ionics 144:123
28. Mitberg EB, Patrakeev MV, Lakhtin AA, Leonidov IA, Kozhevnikov VL, Poeppelmeier KR (1998) J Alloys Compds 274:103
29. van Doorn RHE, Fullarton IC, de Souza RA, Kilner JA, Bouwmeester HJM, Burggraaf AJ (1997) Solid State Ionics 96:1
30. Stevenson JW, Armstrong TR, Carneim RD, Pederson LR, Weber WJ (1996) J Electrochem Soc 143:2722
31. Kruidhof H, Bouwmeester HJM, van Doorn RHE, Burggraaf AJ (1993) Solid State Ionics 63–65:816
32. ten Elshof JA, van Hassel BA, Bouwmeester HJM (1995) Catal Today 25:397
33. Steghuis AG, van Ommen JG, Seshan K, Lercher JA (1997) Stud Surf Sci Catal 107:403